



Study on high-efficiency separation of laminated glass by skillfully combining laser-induced thermal-crack propagation and laser thermal melting

Peng Liu¹ · Leimin Deng¹ · Fei Zhang¹ · Hang Chen¹ · Jun Duan¹ · Xiaoyan Zeng¹

Received: 10 November 2019 / Accepted: 10 March 2020 / Published online: 20 March 2020
© Springer-Verlag GmbH Germany, part of Springer Nature 2020

Abstract

Laminated glass has a wide range of applications, but the cutting process is too cumbersome. In this paper, a novel laser composite separation method was proposed to separate the laminated glass by one time and simplify the cutting process from five steps to two steps for the first time by skillfully combining laser-induced thermal-crack propagation and laser thermal melting. This method generated three laser foci, and each laser focus is acting on one layer of laminated glass. Then, the composite mechanism combining laser-induced thermal-crack propagation for glass layers and laser thermal melting separation for PVB layer was realized to separate entire laminated glass. The experiments of separating laminated glass with thickness of 5 + 0.38 + 5 mm were carried out by laser composite separation successfully, and the separation side wall was very smooth (roughness of glass layer reached 10.24 nm) without any separation defects such as chipping, micro-cracks or subsurface damage. A mathematical model was also established to analyze the separation mechanism.

Keywords Laser separation · Laminated glass · Laser-induced thermal-crack propagation · Laser melting · Numerical simulation

1 Introduction

Laminated glass is usually a sandwich structure composite material, and the typical structure of laminated glass constitutes two float glass layers combined by a PVB (polyvinyl butyral) interlayer [1, 2]. As laminated glass combining the advantages of glass and PVB interlayer, it has the advantages of high strength, no color-fading, fatigue resistance, weathering resistance, and ease of installation [3, 4]. The laminated glass has been widely used as the main safety-protecting materials in construction, auto-industry, marine, aerospace, and military [5–7].

Until now, most of the studies were focused on the failure criteria and damage threshold of laminated glass [8–10], the reinforcement of laminated glass [11, 12], the drilling of laminated glass [13], and so on. However, there is almost no

research on the separation of laminated glass. The existing separating methods of laminated glass are very cumbersome and time-consuming [14]. For example, to obtain a laminated glass with a specific size, the existing cutting method is to separate two pieces of float glass layers and PVB interlayer by mechanical methods, respectively. Then, the two pieces of float glass layers and one piece of PVB interlayer are integrated together under high temperature (temp) or high pressure. Finally, the edges of laminated glass have to be subsequently polished to remove the cutting defects and edge misaligns during the integrated process. In the whole manufacturing process, each step needs to be completed mechanically or manually, which not only increases the manufacturing process, but also consumes much time and man power [15].

Recently, the mechanism of laser-induced thermal-crack propagation (LITP) was used to cut the glass materials [16–18]. This method has been widely used in industrial glass separation with good quality and high speed, like separating mobile glass panels, TV glass panels, float glass, and so on [19–21]. However, the laser used in LITP has only one focus, and the range of laser focusing is limited, resulting in the LITP technology that could only separate thin

✉ Jun Duan
duans@hust.edu.cn

¹ Wuhan National Laboratory for Optoelectronics, Huazhong University of Science and Technology, Wuhan 430074, China

materials. As a result, when separating the laminated glass, the LITP could only separate one layer of laminated glass, and the overall separation of laminated glass could not be completed, resulting in the failure of separation.

A novel separation method—laser composite separation (LCS), of laminated glass was presented in this paper for the first time by skillfully combining the mechanisms of LITP and laser thermal melting. The LCS employs the multi-focus separating head to generate three laser foci on the laser optical axis. By adjusting the parameters of the separating head, each laser focus had a suitable power distribution and acted on the middle part of each layer of laminated glass to achieve overall separation by one time with high quality and did not need any subsequent processing. In this way, the cutting process of laminated glass can be simplified from five steps to two steps (Fig. 1), which improves the production efficiency and eliminates the manufacturing cost. This technology has already been patented, and the related numbers are 201610850924X [22] and ZL 201621080887.0 [23].

2 Basic principle of laser composite separation of laminated glass

The basic principle of laser composite separation of laminated glass is to utilize the multi-focus separating head to generate three laser foci along the thickness direction of laminated glass, and each laser focus is focused on the middle part of each layer of laminated glass, as shown in Fig. 2a.

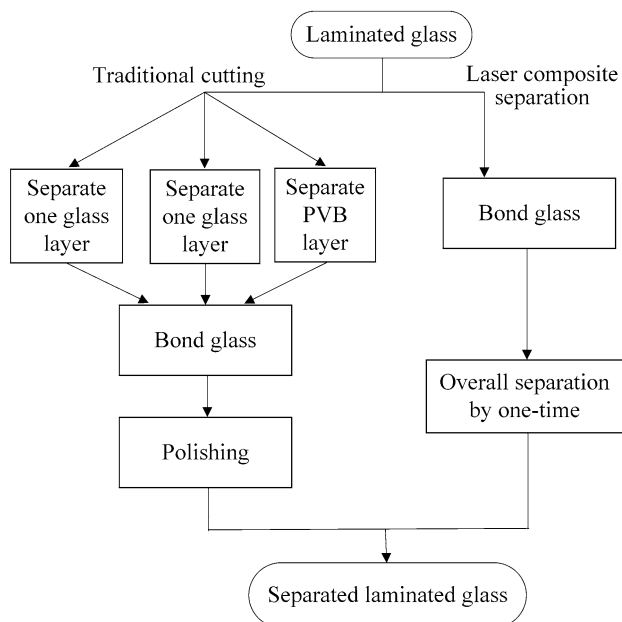


Fig. 1 Comparison of the separation processes between traditional cutting and laser composite separation of laminated glass

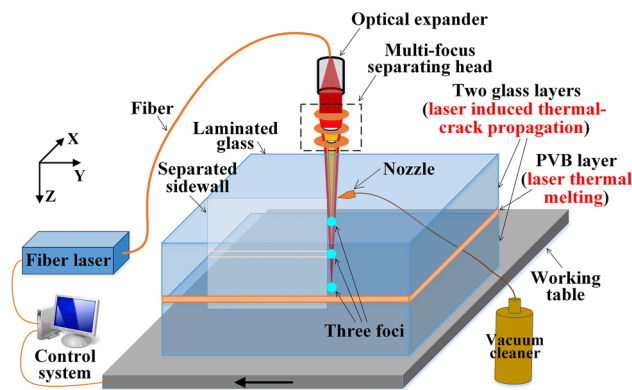


Fig. 2 Diagram of LCS cutting laminated glass

For the two glass layers of laminated glass, the heating of laser foci will cause glass layers to be expanded and the cooling of materials and environment will make the glass layers to be contracted. During the expansion and contraction processes, huge thermal tensile stress will generate and exceed the tensile stress threshold of glass, thereby forming the penetration cracks on glass layers. When the laser beam moves, the penetration cracks would expand forward to accomplish the separation of glass layers. Thus, the glass layers of laminated glass will be separated by the mechanism of LITP. For the PVB layer of laminated glass, the heating of laser focus will generate high temp on the PVB layer, which will exceed the melting point of PVB to accomplish the separation. Thus, the PVB layer will be separated by the laser thermal melting mechanism. Therefore, combining the separation mechanisms of LITP and laser thermal melting, LCS could realize the entire separation of laminated glass by one time. This method not only simplifies the separation process of laminated glass and improves the separation efficiency, but also achieves a good separation quality of laminated glass, and is beneficial to accomplish the automatic separation of laminated glass.

3 Experimental material and equipments

3.1 Material

The laminated glass used in this paper is the commercial laminated glass with size of 200 mm (length) × 100 mm (width) × 10.38 mm (thickness), and the thickness of laminated glass is 5 + 0.38 + 5 mm (5 mm of glass layers and 0.38 mm of PVB layer). In addition, the main physical properties of laminated glass are shown in Table 1.

Table 1 Properties of laminated glass

Properties	PVB layer	Glass layers
Density (kg/m ³)	1100	2480
Specific heat (J/(kg K))	1967	836
Thermal conductivity (W/(m K))	0.2	0.8
Expansion coefficient (×10 ⁻⁶ K ⁻¹)	260	9.1
Poisson's ratio	0.48	0.23
Tensile strength (MPa)	20	30
Compressive strength (MPa)	NA	630
Young's modulus (Pa)	1.49×10 ⁷	7.4×10 ¹⁰
Softening temperature (°C)	60	720
Melting temperature (°C)	175	NA
Burning temperature (°C)	240	NA
Refractive index	1.488	1.516

Table 2 Main parameters of the fiber laser

Parameters	Laser
Wavelength (nm)	1070
Beam quality (M ²)	< 1.05
Max. power (W)	100
Mode of operation	CW
Output power stability (%)	± 0.5
Beam diameter after expansion (mm)	18

3.2 Equipments

The laser used in this paper is a CW fiber laser manufactured by the IPG company (YLS-100), which has a good beam quality and stable power output. In addition, the laser parameters are shown in Table 2.

The multi-focus separating head was utilized to produce three laser foci on the optical axis of laser beam. The multi-focus separating head used in this paper composed of three focusing lenses (Q₁, Q₂, and Q₃), as shown in Fig. 3. The Q₂ and Q₃ have the pores with diameters of D_{p2}, D_{p3} in the center. Moreover, Table 3 shows the meaning of the other symbols.

Table 3 Meaning of symbols of multi-focus separating head

Meaning	Symbols
Diameter of Q ₁₋₃	f ₁₋₃ , respectively
Thickness of Q ₁₋₃	H ₁₋₃ , respectively
Diameter of Q ₁₋₃	D ₁₋₃ , respectively
Thickness of three layers of laminated glass	h ₁₋₃ , respectively
Distance between Q ₁ and Q ₂	l ₁
Distance between Q ₂ and Q ₃	l ₂
Distance between Q ₃ and laminated glass	l ₀
Diameter of incident laser beam	D ₀
Distance between formed laser foci and glass top surface	S ₁₋₃ , respectively

The design of the multi-focus separating head requires reasonable position, and power distributions of laser foci to ensure the separating mechanisms could be effective in LCS. Thus, the ZEMAX software is used to simulate the optical path of multi-focus separating head to obtain the suitable parameters of the optical system. After a series of simulations, the suitable parameters for multi-focus separating head were obtained, as shown in Table 4.

Figure 4 shows the optical paths of the CW fiber laser beam through the designed multi-focus separating head which were simulated by ZEMAX software. The external part of laser beam is refracted three times by Q₁, Q₂, and Q₃ to obtain the shortest focal length and form the focus₁ on the top glass layer of laminated glass (see Fig. 4a). The middle part of laser beam is refracted two times by Q₁ and Q₃ to have the middle focal length and form the focus₂ on the PVB layer of laminated glass (see Fig. 4b). At the same time, the left part of laser beam is refracted one time by Q₁ to have the longest focal length and form the focus₃ on bottom glass layer of laminated glass (see Fig. 4c).

The properties of formed laser foci were calculated through the ZEMAX software [20]. In addition, Table 5 shows the acquired parameters of laser foci (position S_i, power percentage η_i, waist diameter ω_i, divergence half-angles θ_i).

Fig. 3 Diagram of multi-focus separating head

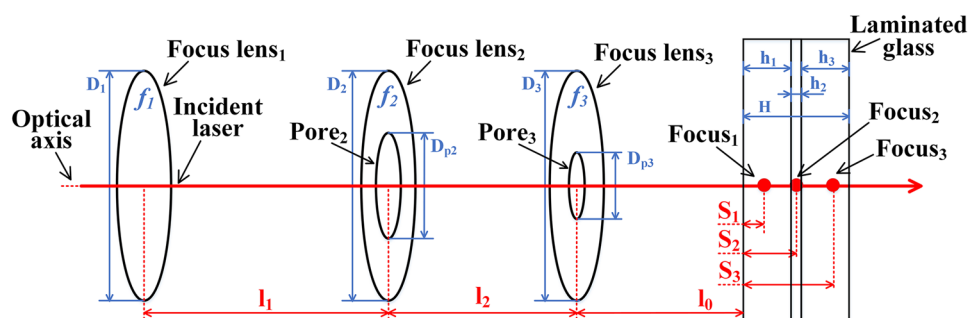


Table 4 Parameters of multi-focus separating head (Unit mm)

	D_0	D_1	D_2	D_3	f_1	f_2
Parameter	18	25.4	25.4	25.4	75	300
	f_3	H_1	H_2	H_3	D_{p2}	D_{p3}
Parameter	125	4.1	2.6	3.3	4.6	2
	l_1	l_2	l_0	h_1	h_2	h_3
Parameter	40.6	9	12.2	5	0.38	5

Fig. 4 Sequential ray tracing models of laser foci. **a** Focus₁. **b** Focus₂. **c** Focus₃

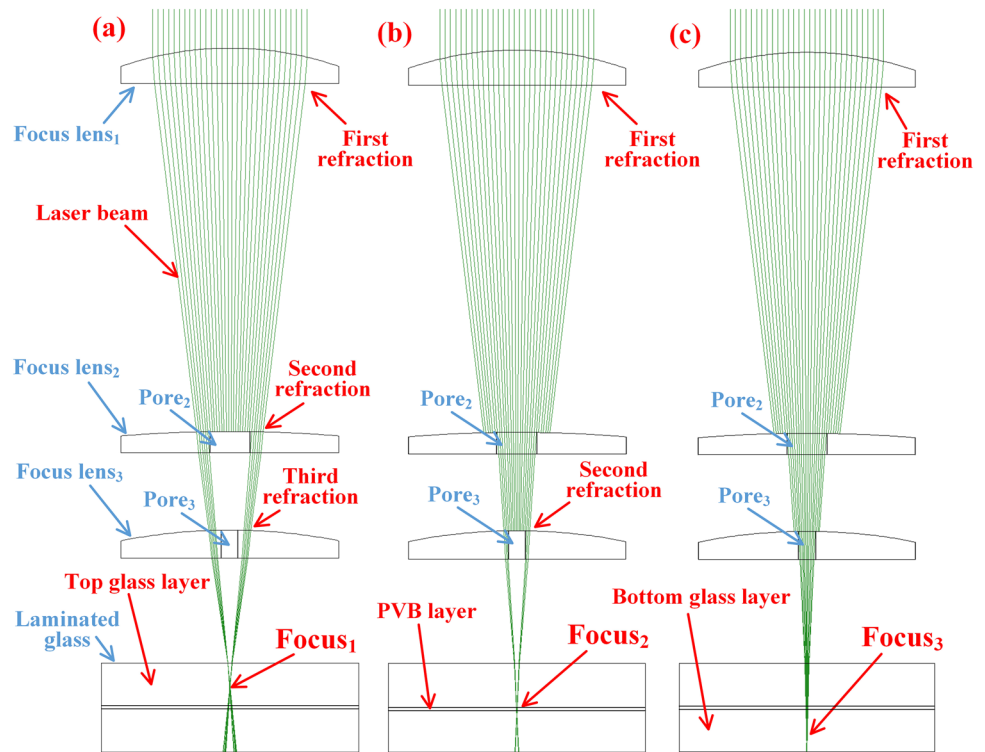


Table 5 Parameters of laser foci

Parameters	Focus ₁	Focus ₂	Focus ₃
S_i (mm)	2.5	5.2	7.8
η_i	36.64%	11.97%	40.38%
ω_i (μm)	3.409	3.694	4.260
θ_i	$0.064 < \theta < 0.077$	$0.049 < \theta < 0.063$	$0 < \theta < 0.042$

The results by the ZEMAX software indicate that three effective laser foci were generated by the multi-focus separating head, and each laser focus acts on one layer of laminated glass, which is the first step to accomplish the separation.

4 Experiments and results

4.1 Processing methods

The experimental platform of LCS was established by the parameters in Tables 1, 2, 3, as shown in Fig. 5. The CW fiber laser was utilized to generate three laser foci through the multi-focus separation head, which were located in the middle part of each layer of laminated glass, respectively. The laminated glass was placed on the 2D moving platform and could be 2D moved on X–Y direction. The control system was used to control the power P as well as the moving speed V of the laser. After the laser was emitted, the platform

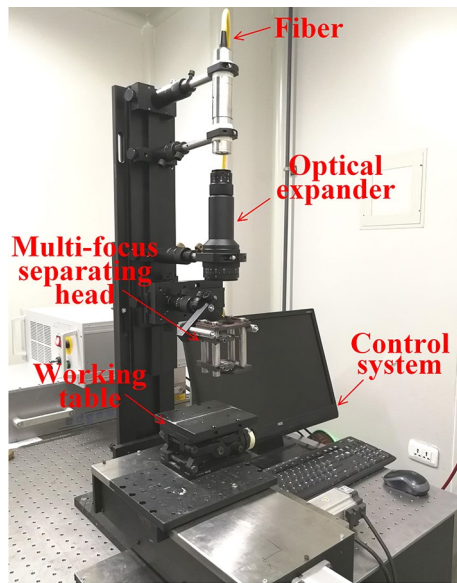


Fig. 5 Established experimental platform

was controlled to move relatively to the laser beam, which made the laser foci acted on the middle part of each layer of laminated glass. After the laser was emitted to the laminated glass, the penetration cracks would be formed on glass layers and expanded forward to trail the laser about 1 mm. Following the movement of laminated glass, penetration cracks expanded forward to complete the cutting of glass layers. Meanwhile, the PVB layer is melted by the laser focus, making the laminated glass separate by LCS by one time. After the experiments, utilize the optical microscopy (Nikon Epi-phot 300) and the scanning electron microscopy (Quanta 3D FEG: SEM/FIB Microscope) to explore the characteristics of separated surfaces and separation side wall. Moreover, the surface morphologies of the separation side wall were examined by a 3D surface profilometer (Veeco Dektak 150) to acquire the roughness.

4.2 Experiments results

When $P = 80$ W and $V = 700$ $\mu\text{m/s}$, laminated glass (5+0.38+5 mm) was separated by LCS successfully. Photomicrographs of front and behind surfaces of laminated glass are shown in Fig. 6. It could be observed that the smooth, clean separation quality was obtained on the front and behind surfaces of laminated glass. In addition, no cutting defects exist, like edge breakage, micro-crack or subsurface damage. Moreover, the very narrow separated kerfs of 68 μm and 61 μm were obtained on the front and behind surfaces of laminated glass, which can be seen in Fig. 6a, b.

Figure 7 shows the morphologies of separation side wall surface of laminated glass ($P = 80$ W, $V = 700$ $\mu\text{m/s}$). The three layers of laminated glass (top glass layer, PVB layer

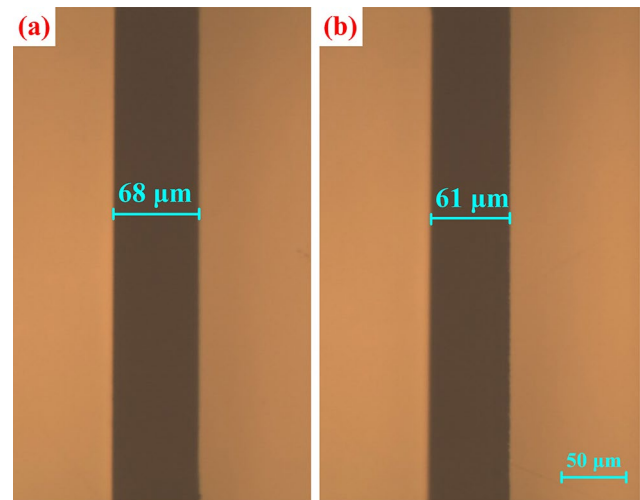


Fig. 6 Photomicrographs of kerfs on the front and behind surfaces of laminated glass separated by LCS. **a** Front surface. **b** Behind surface

and bottom glass layer) were separated neatly, as shown in Fig. 7a. The entire separation side wall is very smooth and clean without any contamination. The optical photomicrographs on the upper and lower ends of separated surface show that the separated edges are very straight and smooth with no ripples, micro-cracks, subsurface damage or other separation defects (see Fig. 7b, c).

Figure 8 shows the observation results with higher magnification of the separation side wall of laminated glass by SEM. Even be enlarged of 2000 \times and 4000 \times , the separated surfaces of glass layers are still smooth without any defects (like ripple or contaminations), indicating the ultra-smooth surfaces were acquired by LCS on glass layers (see Fig. 8a, b). The PVB layer was also observed by the SEM clearly, as shown in Fig. 8c. The PVB layer was separated by LCS neatly and remained obvious vestiges of laser thermal melting, which was coincident with the assumption in Sect. 2, as shown in Fig. 8d. The junctions between glass layers and PVB layer are very straight and smooth, and there are no ripples, micro-cracks, subsurface damage, pollution or other separation defects on the glass layers, indicating the melting of PVB layer has little effect on the separation of glass layers of laminated glass, as shown in Fig. 8c. The results of optical microscopy and SEM indicate an excellent separation quality was obtained on the separation edges of laminated glass.

Moreover, Fig. 9 shows the undulation of separation surface by the 3D surface profilometer. The measuring results show that the fluctuations of the two glass layers are very little (only dozens of nanometers), and the roughness of the top and bottom glass layers (position A and position C in Fig. 8a, respectively) is ($R_a = 10.24$ nm, $R_p = 55.65$ nm, $R_t = 6.66$ nm, $R_{\text{max}} = 104.64$ nm) and ($R_a = 11.21$ nm, $R_p = 72.72$ nm, $R_t = 42.57$ nm, $R_{\text{max}} = 102.87$ nm), respectively, as shown in

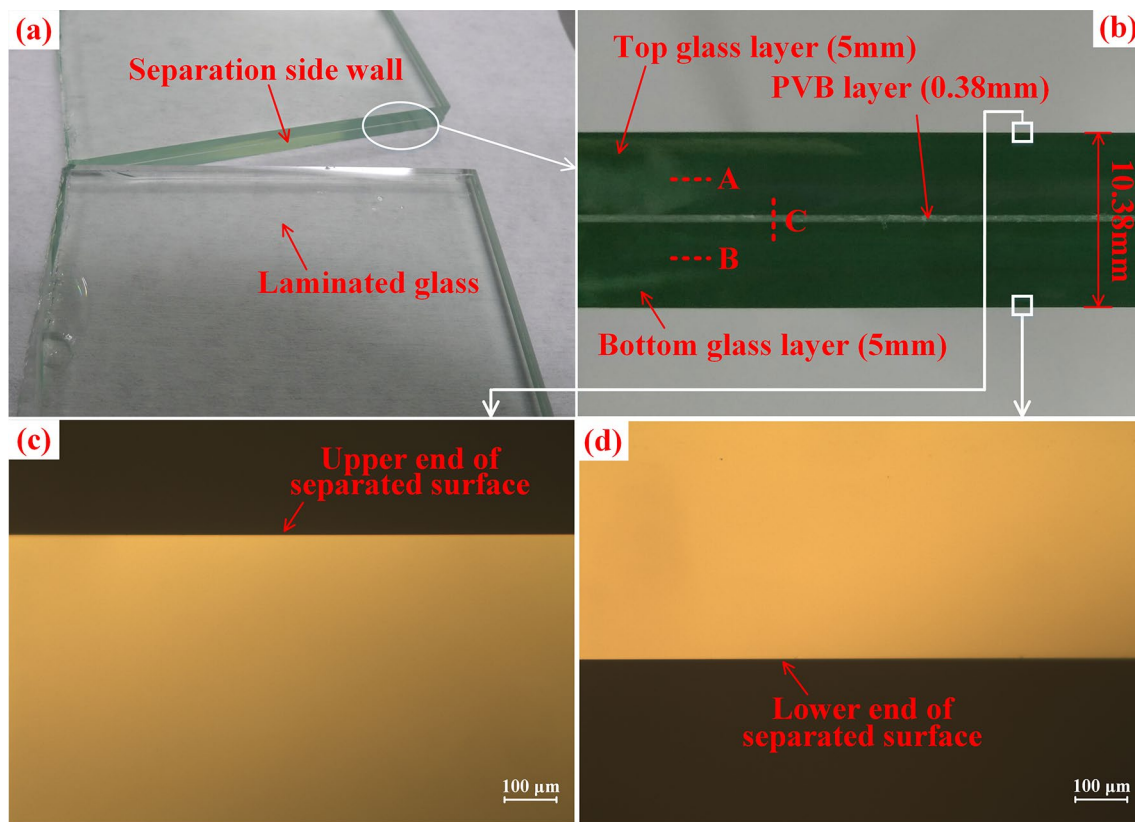


Fig. 7 Separation side wall of laminated glass. **a** Overall view of separation side wall. **b** Optical photomicrograph of upper end of separated surface. **c** Optical photomicrograph of lower end of separated surface

Fig. 9a, b. The measuring results indicate that the separation side walls of two glass layers are extremely smooth, which are coincident with the results of photomicrographs in Figs. 7, 8. Moreover, the measuring results of PVB layer (position C in Fig. 8a) indicate that the laser thermal melting of PVB layer produced some fluctuations on PVB layer. The maximum fluctuation of PVB layer is only about 50 μm , which is good enough for PVB materials to be applied in practical industries, as shown in Fig. 9c.

The detecting results demonstrate that an excellent separation quality of laminated glass could be obtained by LCS, and the separated laminated glass could be used in industrial applications directly without any subsequent process.

In contrast, the conventional mechanical separation methods have poor separation quality on separation side wall with cracks, underground damages as well as obvious tear marks, as shown in Fig. 10a. The enlarged optical photomicrograph of the separation side walls shows the poor separation quality clearly, and the roughness (R_a) of the laminated glass separated by traditional mechanical method was 34.03 μm , as shown in Fig. 10b. Therefore, in terms of separation quality, the LCS of laminated glass has great advantages. Moreover, the LCS simplifies the separation process greatly compared to the conventional mechanical separating method

of laminated glass. Thus, it could be said that the LCS of laminated glass has great advantages than the conventional mechanical separating methods.

In addition, when cutting laminated glass with more layers, such as military bullet-proof laminated glass with five layers, the optical path should be adjusted by increasing the quantity of the focusing lenses (like Q_4 , Q_5 , and so on) in multi-focus separating head, thereby adding the quantity of laser foci, and completing the separation of laminated glass with more layers.

Moreover, the LCS has versatile field of manufacturing the composite materials with similar structures, such as solar panels and liquid crystal display panels, which will be studied in our subsequent researches. Thus, the LCS has great practical application prospects and scientific value.

5 Numerical simulation and discussion

Since the separation mechanism of LCS was LITP and laser thermal melting, distributions of temp and thermal stress in laminated glass in the cutting process are very important to accomplish the separation. In this section, the finite element analysis method was employed to analyze the distributions

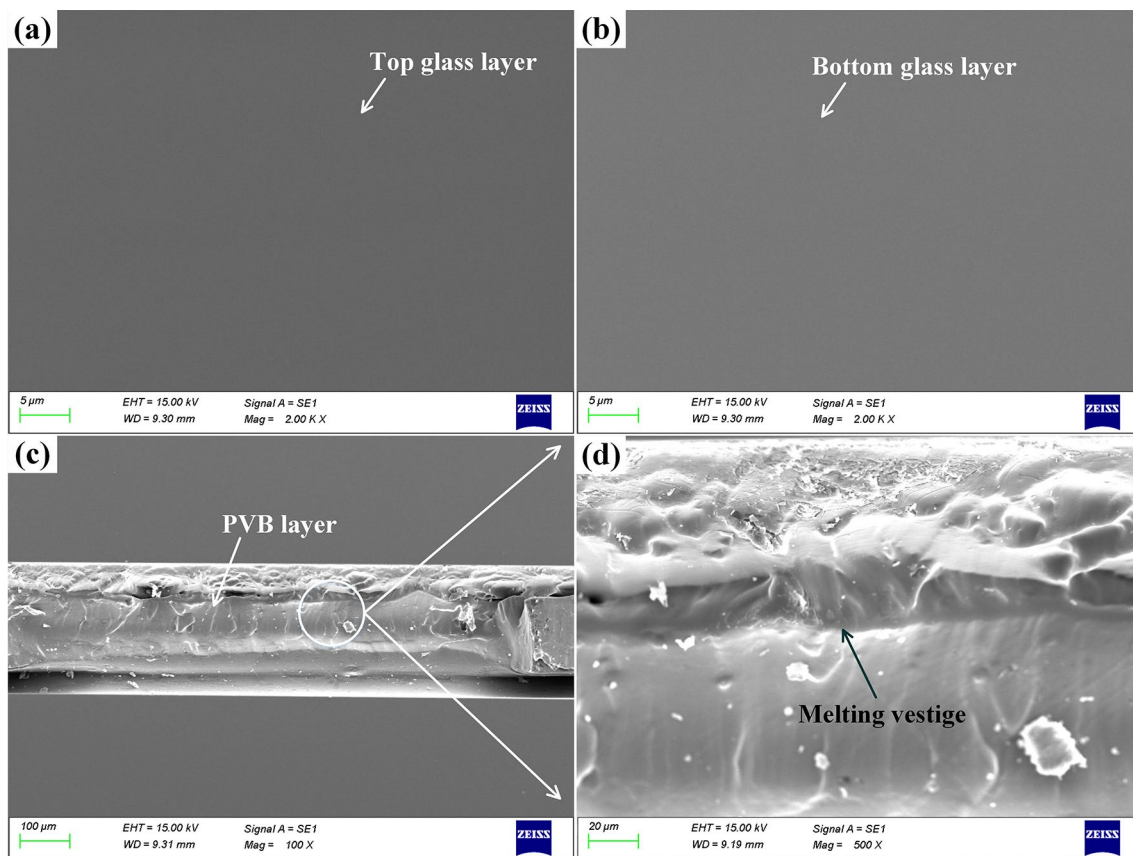


Fig. 8 Morphologies of separation side wall by SEM. **a** Morphology of top glass layer. **b** Morphology of bottom glass layer. **c** Morphology of PVB layer. **d** Enlarged morphology of PVB layer

of temp and thermal stress in laminated glass to have a comprehensive understanding of the separation mechanism of LCS with ANSYS software.

5.1 Mathematical model

The mathematical model of laser foci in LCS is established based on the designed multi-focus separating head (Sect. 3.2). And the meaning of the symbols in the mathematical model is listed in Table 6.

The zero point of Z-axis is set on the front surface of laminated glass. On front surface of laminated glass, the distributions of the amplitude of laser beam i could be described by the following formula.

$$E(x, y, z, t) = \frac{\sqrt{\frac{2P}{\pi}}}{\omega(z)} e^{-\frac{r^2}{\omega^2(z)}} e^{-i \left[k \left(z - s_i + \frac{r^2}{2(z - s_i + \frac{r^2}{z - s_i})} \right) - \arctan \left(\frac{z - s_i}{f} \right) \right]}, \quad i = 1, 2, 3 \tag{1}$$

where

$$\begin{cases} r = \sqrt{x^2 + (y - Vt)^2} \\ f = \frac{\pi \omega_i^2}{\lambda} \\ k = \frac{2\pi}{\lambda} \end{cases} \tag{2}$$

The diffraction integral of laser spot pattern on laminated glass front surface would produce laser focus_i inside the laminated glass. As a result, the amplitude distribution inside the laminated glass could be described by the following formula. (To simplify the calculation, the optical properties of PVB layer are considered to be same with the optical properties of glass layers.)

$$E_{LG}(x, y, z, t) = \frac{1}{4\pi} \iint_{\Sigma} \left[\frac{\partial E}{\partial \vec{d}} \left(\frac{e^{ikn \vec{s}}}{\vec{s}} \right) - E \frac{\partial}{\partial \vec{d}} \left(\frac{e^{ikn \vec{s}}}{\vec{s}} \right) \right] d\sigma \tag{3}$$

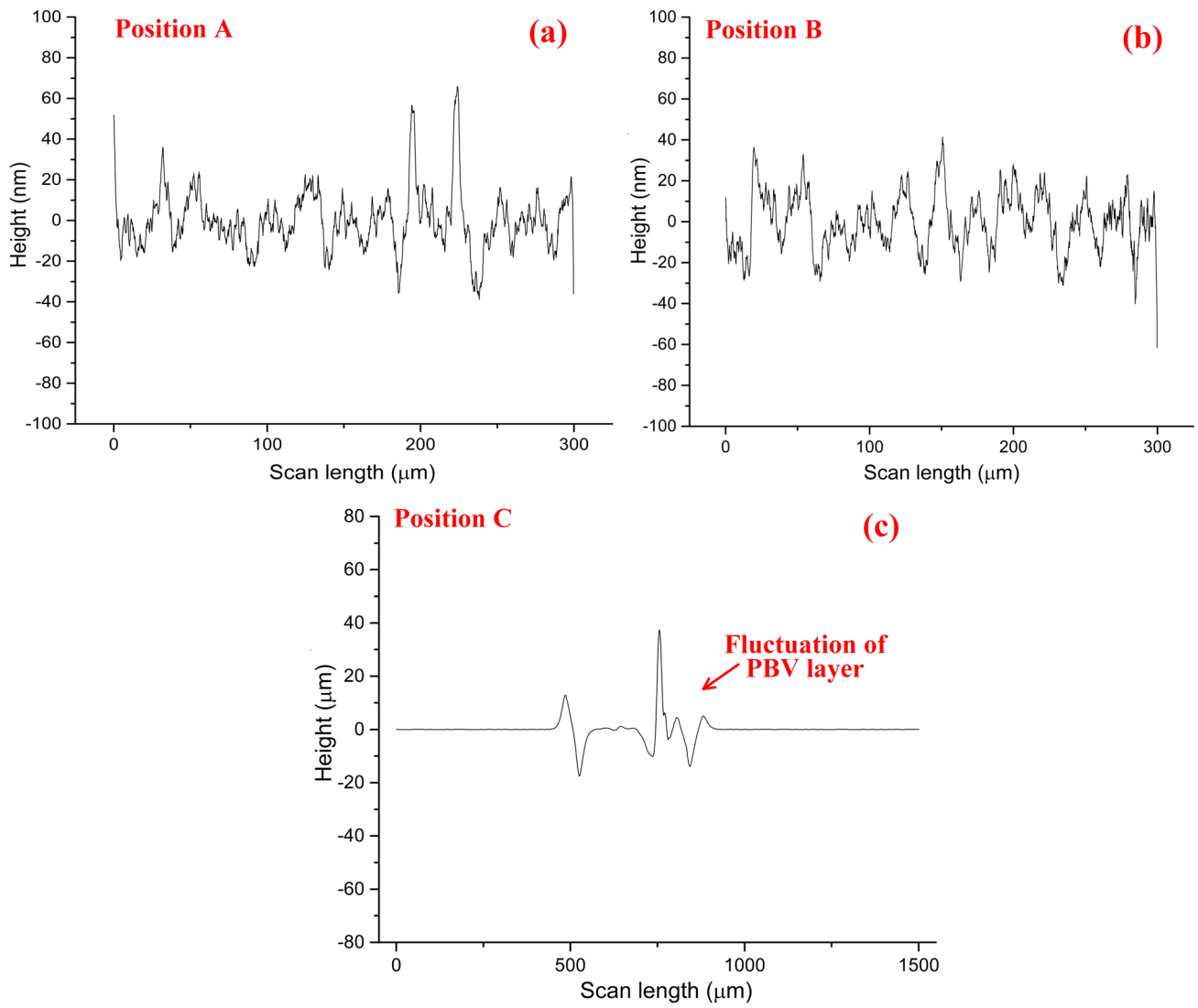


Fig. 9 3D surface measuring results of different positions on separation side wall. **a** Position A. **b** Position B. **c** Position C

Fig. 10 Separation morphologies of traditional mechanical separating methods of laminated glass. **a** Overall view. **b** Optical photomicrograph

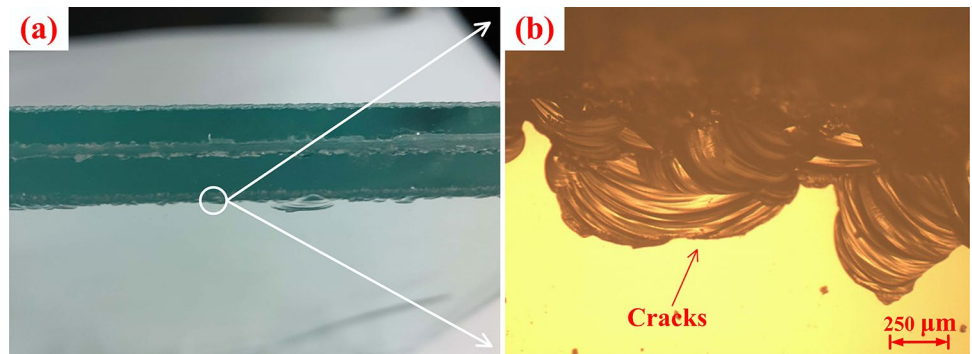


Table 6 Meaning of symbols in mathematical model

Meaning	Symbols
Laser spot pattern on front surface of laminated glass	Σ
Normal vector of laminated glass front surface	\vec{d}
Vector from integral point to (x, y, z) point	\vec{s}
Refractive index of laminated glass	n
Density of glass layers	ρ_g
Density of PVB layer	ρ_p
Specific heat of glass layers	C_g
Specific heat of PVB layer	C_p
Temp of laminated glass	T
Thermal conductivity of glass layers	k_g
Thermal conductivity of PVB layer	k_p
Convection coefficient between laminated glass and air	h_c (12.5 W m ² K ⁻¹)
Temp of surrounding environment	T_{air} (25 °C)
Laser light intensity distribution of focus _{<i>i</i>}	$I_i(x, y, z, t)$
Divergence half-angle of laser beam at point (x, y, z)	$\theta_i(z)$
Absorption rate of glass layers of 1070 nm wavelength laser	η_0
Absorption rate of PVB layer of 1070 nm wavelength laser	η_1

As a result, laser light intensity distributions of focus_{*i*} ($I_i(x, y, z, t)$) in the laminated glass could be described by the following formula.

$$I_i(x, y, z, t) = E_{LG}^2 \tag{4}$$

At the same time, on laminated glass front surface, the laser beams' divergence half-angle ranges were utilized to calculate the spot pattern.

$$\begin{cases} \theta_i(z) = \arctan\left(\frac{\omega_i(z)}{\text{abs}(z-S_i)}\right), & i = 1, 2, 3 \\ 0.064 < \theta_1(z) < 0.077 \\ 0.049 < \theta_2(z) < 0.063 \\ 0 < \theta_3(z) < 0.042 \end{cases} \tag{5}$$

Moreover, each laser focus_{*i*} could produce a heat intensity distribution Q_i inside the laminated glass, which could be described by the following formula.

$$\begin{cases} Q_i(x, y, z, t) = -\frac{\partial}{\partial z} I_i e^{-\eta_0 z}, & i = 1, 3 \\ Q_i(x, y, z, t) = -\frac{\partial}{\partial z} I_i e^{-\eta_1 z}, & i = 2 \end{cases} \tag{6}$$

The heat source functions of the three laser foci beams inside the laminated glass could be calculated by Formulas (1)–(6).

The 3D heat conduction equations were utilized to describe the thermal spread process of the laminated glass.

$$\begin{cases} \rho_g C_g \frac{\partial T(x, y, z)}{\partial t} = k_g \left(\frac{\partial^2 T}{\partial^2 x} + \frac{\partial^2 T}{\partial^2 y} + \frac{\partial^2 T}{\partial^2 z} \right) + Q_i(x, y, z, t), \\ \quad (i = 1, 2, 3, \quad 0 < z < 5 \text{ mm} \ \& \ 5.38 \text{ mm} < z < 10.38 \text{ mm}); \\ \rho_p C_p \frac{\partial T(x, y, z)}{\partial t} = k_p \left(\frac{\partial^2 T}{\partial^2 x} + \frac{\partial^2 T}{\partial^2 y} + \frac{\partial^2 T}{\partial^2 z} \right) + Q_i(x, y, z, t), \\ \quad (i = 1, 2, 3, \quad 5 \text{ mm} < z < 5.38 \text{ mm}); \\ T(x, y, z, 0) = 298.15; \\ -k \frac{\partial T}{\partial n} \Big|_{\Sigma} = h_c(T - T_{air}); \end{cases} \tag{7}$$

The finite element analysis was carried out by the ANSYS software. In the simulation process, we selected element SOLID 5 to do the thermal analysis and element SOLID 226 to do the thermal stress analysis. Moreover, the adhesive force was simulated by contact element pairs TARGE 170 and 174 with thermal conductivity of 20%. In the simulation process, the laminated glass was glued as a whole. The maximum normal stress theory was used to simulate the glass tensile failure and the emergence of the cracks. When the thermal tensile stress generated by the laser foci in glass layers was greater than the tensile stress threshold of glass materials, the cracks would emerge and the corresponding finite elements would be deleted.

The established simulation model is shown in Fig. 11. The laser acting regions are fine-meshed, and the surrounding

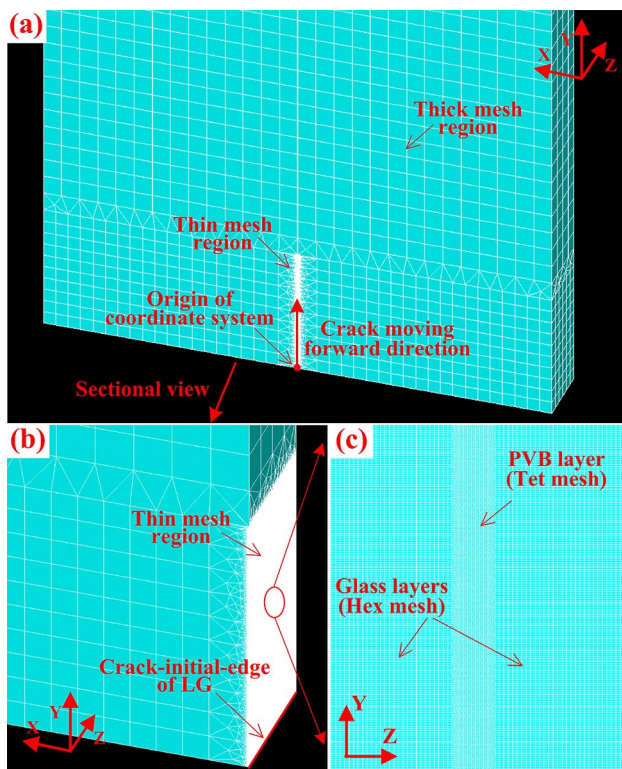


Fig. 11 Established finite element model. **a** Overall view. **b** Sectional view. **c** Enlarged view of the mesh of PVB layer and glass layers

regions are thick-meshed, which is connected via free tet, as shown in Fig. 13a, b. The PVB layer of laminated glass was meshed by free tet, and the laser acting regions of glass layers were meshed by hex. In addition, the meshing size of laser acting regions is $20 \times 40 \times 100 \mu\text{m}$ (see Fig. 13c). This modeling method could guarantee the simulation accuracy and reduce the calculation time.

5.2 Simulation results

The process of LCS cutting laminated glass was simulated ($P=80 \text{ W}$, $V=700 \mu\text{m/s}$, and see Tables 1, 2, 3, 4, 5 for other parameters). The temp and thermal stress distributions at different moments are shown in Figs. 12, 13.

When $t=0.4 \text{ s}$, the laser beam enters the crack-initial-edge of laminated glass and heats the three layers of laminated glass simultaneously. As a result, three red dot-like high temp regions formed on the laminated glass thickness direction, as shown in Fig. 12a. For the two glass layers of laminated glass, the top and bottom glass layers are heated by the two laser foci, respectively, resulting in an increase in temp. This high temp could not cause damages to the glass layers as the highest temp generated (about $130 \text{ }^\circ\text{C}$) is inferior to glass softening temp ($720 \text{ }^\circ\text{C}$), which can be seen in Fig. 12b. On X-direction of two glass layers, the

increase in temp makes the glass layers thermal expansion, but they were restricted by the surrounding materials, thus generating a huge thermal compressive stress, which can be seen in Fig. 12c. This thermal compressive stress could not cause damages to the glass layers as the biggest stress generated (about 36 MPa) is inferior to glass compressive stress threshold (630 MPa), which can be seen in Fig. 12d. And for the PVB layer of laminated glass, the temp on the PVB layer was about $210 \text{ }^\circ\text{C}$, which is higher than the melting temp of PVB material ($175 \text{ }^\circ\text{C}$) and lower than the burning temp of PVB material ($240 \text{ }^\circ\text{C}$), resulting in the PVB layer being separated by the laser thermal melting, as shown in Fig. 12a, b. Thus, the PVB layer was separated directed by the high temp at the beginning of separation.

After a period of time and when $t=1.9 \text{ s}$, fiber laser moves ahead about 0.7 mm , and the high temp regions move ahead accompanying the laser beam synchronously, as shown in Fig. 13a. For the two glass layers of laminated glass, with the leave of laser beam and the heat exchanges between materials and environment, the temp of crack-initial-edge drops, as shown in Fig. 13b. On the X-direction of two glass layers, the drop of temp changing the thermal expansion phenomenon as contraction phenomenon, which leads to the thermal compressive stress, is also transformed to thermal tensile stress (see Fig. 13c). This tensile stress is higher than glass tensile stress threshold (29 MPa), which can be seen in Fig. 13d. In consequence, the penetration cracks would be generated on two glass layers of laminated glass along thickness direction. With the movement of the laser beam, the penetration cracks will expand ahead along the path of laser beam until the two glass layers are cut entirely, as shown in Fig. 14. As PVB layer of laminated glass has been separated by the laser thermal melting already, the three layers of laminated glass would be separated by the LCS technology by one time.

Therefore, the simulation results indicated that the LCS technology generated three effective laser foci and separated the three layers of laminated glass, respectively, by two mechanisms (LITP and laser thermal melting, respectively) to separate the laminated glass by one time. These simulation results were coincident with the results of experiments (Sect. 4) and proved the feasibility of LCS, further.

6 Conclusion

In this study, a novel method—laser composite separation, was proposed to separate the laminated glass by one time for the first time in this paper. Through a series of practical experiments and mathematical simulations, it was proved that the two glass layers and one PVB layer of laminated glass were separated by two different mechanisms—laser-induced thermal-crack propagation and laser thermal melting

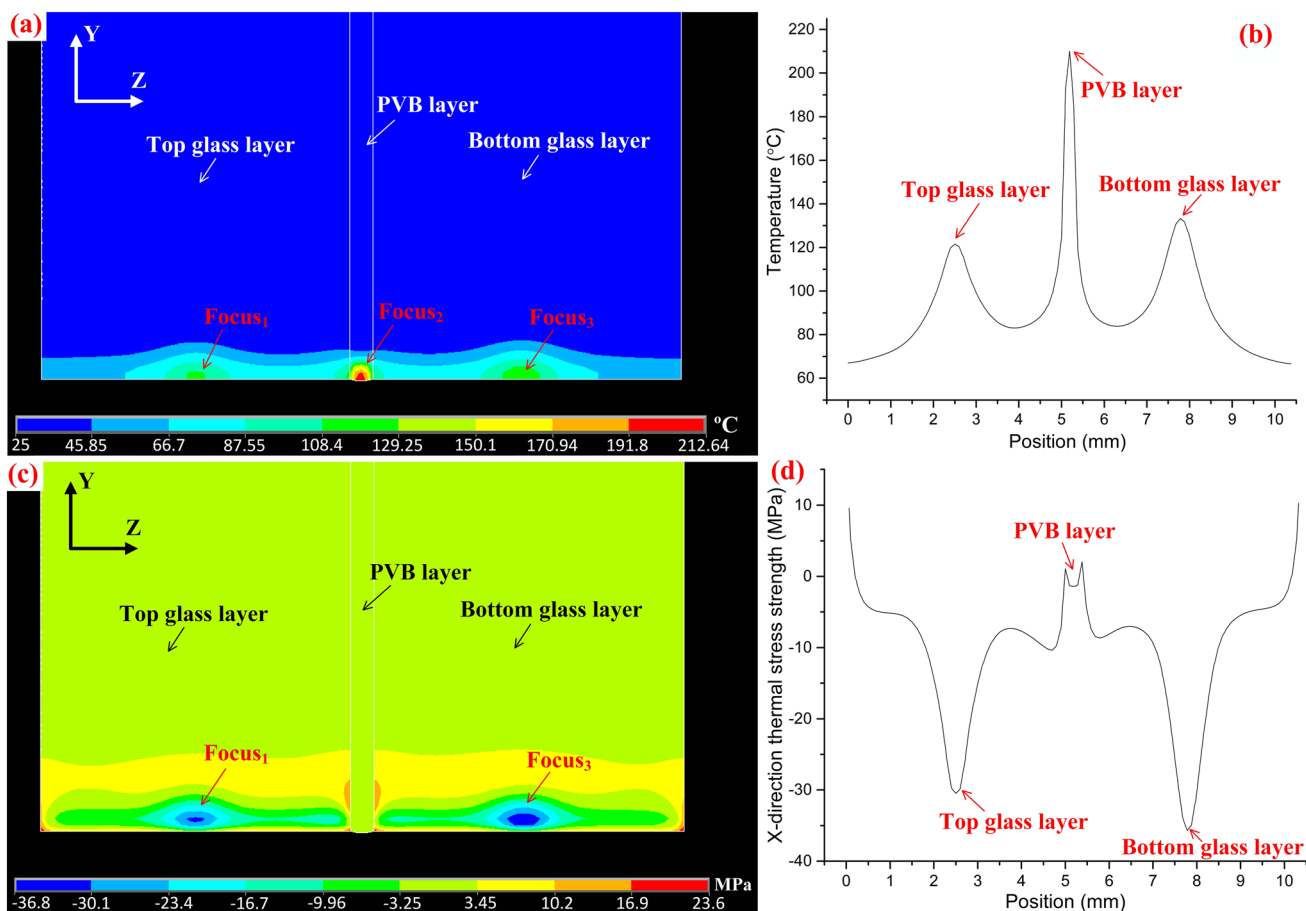


Fig. 12 Distributions of temp and thermal stress of laminated glass separated by LCS when $t=0.4$ s. **a** Temp distribution of separation side wall. **b** Temp distribution of crack-initial-edge. **c** Thermal stress

distribution of separation side wall. **d** Thermal stress distribution of crack-initial-edge

to complete the one-time overall separation of laminated glass, respectively. This technology has greatly improved the production efficiency of laminated glass by simplifying the manufacturing process from five steps (traditional cutting method) to only two steps. Thereby, the laser composite separation reduced the production cost of laminated glass and improved the production efficiency to expand the application ranges of laminated glass. At the same time, the laminated glass separated by laser composite separation has

a good separation quality without any cutting defects, and the surface roughness of the separation side wall of glass layer of laminated glass reached 10.24 nm, indicating the separated laminated glass could be applied to industrial applications without any subsequent processes. Moreover, the mathematical analysis by the finite element simulation was coincident with the practical experiments, which proved the feasibility of the laser composite separation, further.

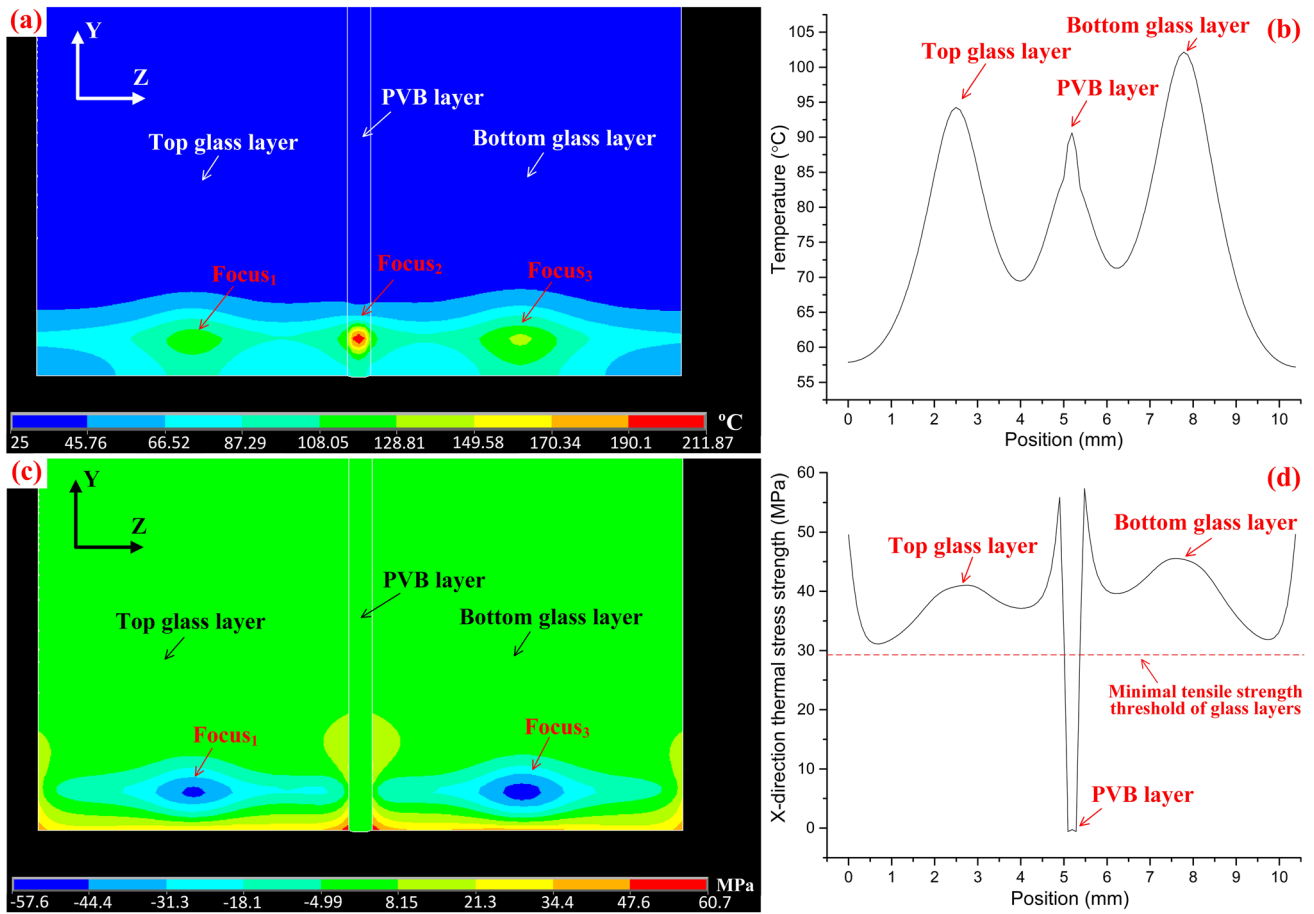


Fig. 13 Distributions of temp and thermal stress of laminated glass separated by LCS when $t=1.9$ s. **a** Temp distribution of separation side wall. **b** Temp distribution of crack-initial-edge. **c** Thermal stress

distribution of separation side wall. **d** Thermal stress distribution of crack-initial-edge

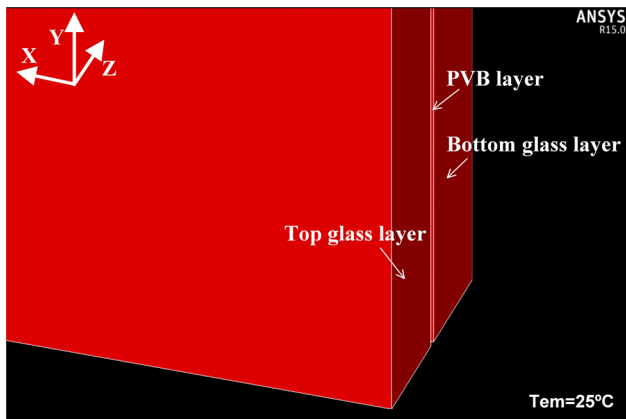


Fig. 14 Laminated glass separated by LCS entirely (distribution of temp)

Acknowledgements The authors gratefully acknowledge the financial supports by the National Natural Science Foundation of China (Nos. 51675205 and 51475182).

References

1. A. Fam, S. Rizkalla, Structural performance of laminated and unlaminated tempered glass under monotonic transverse loading. *Constr. Build. Mater.* **20**(9), 761–768 (2006)
2. P. Foraboschi, Behavior and failure strength of laminated glass beams. *J. Eng. Mech.* **133**(12), 1290–1301 (2007)
3. R. Montanini, F. Freni, Non-destructive evaluation of thick glass fiber-reinforced composites by means of optically excited lock-in thermography. *Compos. Part A Appl. Sci. Manuf.* **43**(11), 2075–2082 (2012)

4. L. Valarinho, J.R. Correia, M.M. Costa et al., Lateral-torsional buckling behaviour of long-span laminated glass beams: analytical, experimental and numerical study. *Mater. Des.* **102**, 264–275 (2016)
5. I. Mohagheghian, M.N. Charalambides et al., Effect of the polymer interlayer on the high-velocity soft impact response of laminated glass plates. *Int. J. Impact Eng.* **120**, 150–170 (2018)
6. E.P. Gellert, D.M. Turley, Seawater immersion ageing of glass-fiber reinforced polymer laminates for marine applications. *Compos. Part A Appl. Sci. Manuf.* **30**(11), 1259–1265 (1999)
7. M. Amin Samieian, D. Cormie et al., Temperature effects on laminated glass at high rate. *Int. J. Impact Eng.* **111**, 177–186 (2018)
8. A. de Souza, G.F. Gomes, E.P. Peres et al., A numerical-experimental evaluation of the fatigue strain limits of CFRP subjected to dynamic compression loads. *Int. J. Adv. Manuf. Technol.* **103**, 219 (2019)
9. X.H. Zhang, H. Hao, G.W. Ma, Parametric study of laminated glass window response to blast loads. *Eng. Struct.* **56**, 1707–1717 (2013)
10. M. Larcher, M. Teich, N. Gebbeken et al., Simulation of laminated glass loaded by air blast waves. *Appl. Mech. Mater.* **82**, 69–74 (2011)
11. A. Warriar, A. Godara, O. Rochez, L. Mezzo, F. Luizi, L. Gorbatiikh, S.V. Lomov, A.W. VanVuure, I. Verpoest, The effect of adding carbon nanotubes to glass/epoxy composites in the fibre sizing and/or the matrix. *Compos. Part A Appl. Sci. Manuf.* **41**(4), 532–538 (2010)
12. Z. Feng, X. Wang, J. Huang et al., Experimental and numerical study of optimum thickness of porous silica transition layer in aeronautic laminated glass. *Mater. Des.* **121**, 367–372 (2017)
13. C.L. Tan, A.I. Azmi, Analytical study of critical thrust force for on-set delamination damage of drilling hybrid carbon/glass composite. *Int. J. Adv. Manuf. Technol.* **92**, 929 (2017)
14. X. Centelles, J. Ramon Castro, Luisa F. Cabeza, Experimental results of mechanical, adhesive, and laminated connections for laminated glass elements—a review. *Eng. Struct.* **180**, 192–204 (2019)
15. G. Tunker, Process for producing a laminated glass pane, especially for a motor vehicle. United States Patent, US005443669A (1995)
16. C.Y. Zhao, H.Z. Zhang, L.J. Yang, Y. Wang, Y. Ding, Dual laser beam revising the separation path technology of laser induced thermal-crack propagation for asymmetric linear cutting glass. *Int. J. Mach. Tools Manuf.* **106**, 43–55 (2016)
17. Y.C. Cai, M.L. Wang, H.Z. Zhang et al., Laser cutting sandwich structure glass–silicon–glass wafer with laser induced thermal-crack propagation. *Opt. Laser Technol.* **93**(1), 49–59 (2017)
18. L.J. Yang, Y. Wang, Z.G. Tian, N. Cai, YAG laser cutting soda-lime glass with controlled fracture and volumetric heat absorption. *Int. J. Mach. Tools Manuf.* **50**, 845–859 (2010)
19. J.K. Jiao, X.B. Wang, Cutting glass substrates with dual-laser beams. *Opt. Laser Technol.* **47**(7–8), 860–864 (2009)
20. P. Liu, J. Duan, B.Y. Wu, L.M. Deng, Y. Shangguan, X.Y. Zeng, X.Z. Wang, A flexible multi-focus laser separation technology for thick glass. *Int. J. Mach. Tools Manuf.* **135**, 12–23 (2018)
21. L.M. Deng, H. Yang, X.Y. Zeng, B.Y. Wu, P. Liu, X.Z. Wang, J. Duan, Study on mechanics and key technologies of laser non-destructive mirror-separation for KDP crystal. *Int. J. Mach. Tools Manuf.* **94**, 26–36 (2015)
22. J. Duan, P. Liu, L.M. Deng, X.Y. Zeng, A method and device for multi-focus laser separating laminated glass, In: S.I.P.O. P.R.C. (Ed.) State Intellectual Property Office of the P.R.C., China (2016)
23. J. Duan, P. Liu, L.M. Deng, X.Y. Zeng, A device for multi-focus laser separating laminated glass, In: S.I.P.O. (Ed.) State Intellectual Property Office of the P.R.C., China (2016)

Publisher's Note Springer Nature remains neutral with regard to jurisdictional claims in published maps and institutional affiliations.